Assessment of earthquake-induced landslide hazard in Greece: From Arias Intensity to spatial distribution of slope resistance demand

Konstantinos Chousianitis[1], Vincenzo Del Gaudio[2], Nikolaos Sabatakakis[3], Katerina Kavoura[3], George Drakatos[1], George D. Bathrellos[4], Hariklia D. Skilodimou[4]

[1] Institute of Geodynamics, National Observatory of Athens, Lofos Nymfon, 11810 Athens, Greece

[2] Dipartimento di Scienze della Terra e Geoambientali, Università degli Studi di Bari, via E. Orabona 4, 70125, Bari, Italy

[3] Laboratory of Engineering Geology, Department of Geology, University of Patras, 26500, Patras, Greece

[4] Department of Geography, Faculty of Geology and Geoenvironment, National and Kapodistrian University of Athens, University Campus, 15784, Zografou, Athens, Greece

Published on Bulletin of Seismological Society of America, doi: 10.1785/0120150172

Abstract

Earthquake shaking can trigger a large number of landslides in hilly or mountainous areas, considerably aggravating the impact of the seismic event in terms of overall damage and loss of life. Thus, the delineation of slope areas that have a significant probability of failing under future seismic action appears imperative for disaster mitigation. In the present study, we follow a time probabilistic approach for the evaluation of earthquake-induced landslide hazard in Greece through the estimation of the minimum resistance required for slopes to remain within a prefixed value of exceedance probability of failure. Taking into account the characteristics of seismicity affecting Greece, we constructed maps representing the spatial distribution of critical acceleration values that imply a 10% probability that Newmark's displacement will exceed significant thresholds in a time interval of 50 years. These maps provide the spatial distribution of the strength demand required for slopes to resist failures under the action of the regional seismicity. Such maps allow an assessment of whether particular slopes have a significant failure probability by comparing the strength demand estimated at the location of the slope with its actual critical acceleration calculated from slope material properties and slope angle. To exemplify the possible use of these strength demand maps in local hazard estimates, we compare, within a GIS framework, the critical acceleration values obtained by the application of the time probabilistic approach with actual in situ critical acceleration values for a coastal area of the Western Gulf of Corinth.

Introduction

It is widely recognized that landslides are one of the most damaging collateral effects associated with seismic shaking within a certain distance from the seismogenic source. In many seismically active areas of the world, earthquake-induced landslides commonly account for a significant portion of the total impact of earthquakes, considerably enhancing their effects in terms of human life and economic losses. Appropriate land use planning as well as civil protection measures could contribute to earthquake-induced landslide hazard mitigation, but they should first evaluate where earthquake-induced landslides are most likely to occur in scenarios expected for future events. Towards this goal, it is of great importance the assessment of areas exposed to slope destabilisation phenomena under seismic shaking through procedures of earthquake-induced landslide hazard evaluation at regional scale.

Keefer (1984) proposed magnitude thresholds for earthquakes to induce landslides and presented a set of upper bound curves for the maximum distance of seismically induced landslides as a function of magnitude. In the same study, seismically-induced landslides were classified into three groups on the basis of movement type and geological environment, namely i) rock falls and disrupted soil slides, ii) coherent deep-seated slides and iii) lateral spreads and flows. The limit curves proposed by Keefer (1984) were subsequently updated by Rodriguez *et al.* (1999). Such kind of curves provides a first tool to delimit the area potentially exposed to slope destabilisation in the framework of an earthquake scenario.

A second, but still simplified, level of regional scale hazard evaluation consists of calculating shaking expected on slopes for a credible earthquake scenario and comparing such shaking with some critical thresholds for seismic-landslide triggering. Wilson and Keefer (1985) proposed the examination of Arias intensity, which quantifies the ground motion energy, and Newmark's displacement, which estimates the permanent coseismic displacement along a slide surface (Newmark*,* 1965). Arias intensity is defined as the energy per unit weight transmitted by seismic ground motion to a set of single-degree-of-freedom oscillators with eigenfrequencies from zero to infinity (Arias*,* 1970). It is calculated from the integral of the acceleration squared over the time, thus it provides a more complete information on total shaking energy in comparison to other scalar parameters (e.g., peak ground acceleration) and shows a better correlation with permanent ground deformation effects produced by earthquakes (cf. Harp and Wilson, 1995). To characterize the shaking energy at a site, one can use the Arias intensity I_α calculated on the largest of the ground motion components or the sum I_h of the two horizontal components (Harp and Wilson, 1985). Keefer and Wilson (1989) defined I_α values of 0.11 m/s as shaking threshold for triggering falls, disrupted slides, and rock avalanches (i.e., incoherent landslides), 0.32 m/s for slumps, block slides, and slow earth flows (i.e., coherent landslides) and 0.54 m/s for lateral spreads and flows.

In a rigorous analysis, Newmark displacement D_n is expressed as the block cumulative permanent displacement of a landslide, modeled as a rigid friction block resting on a slope, as effect of an earthquake. It is calculated through a double integration of the earthquake acceleration-time history restricted to the time intervals when a critical acceleration α_c is exceeded. Wilson and Keefer (1985) suggested that D_n thresholds can be defined, whose exceedance imply a critical drop of shear strength that would induce a slope failure.

More rigorous methods of hazard evaluation at a regional scale have also been developed, providing the basis for a preliminary identification of areas exposed to seismic slope failures. Such methods include the prediction of slope failure probabilities from the estimate of Newmark displacements for a shaking scenario of interest, as well as pseudo-probabilistic and fully probabilistic approaches. With regard to the first approach, Jibson *et al.* (2000), using data from the Northridge earthquake and a Weibull model, yielded a regression equation that links the probability of failure with the estimates of Newmark displacement expected and can be used in any ground-shaking condition. As a step forward, Del Gaudio *et al.* (2003), Rathje and Saygili (2008) and Saygili and Rathje (2009) developed probabilistic frameworks to evaluate the recurrence time of earthquake-induced landslide triggering and are primarily based on the estimation of the sliding displacement hazard curve providing the mean annual rate of exceedance for different displacement levels. The approach of Del Gaudio *et al.* (2003) takes into account the characteristics of the seismicity of a given area and estimates the resistance required for slopes to keep their failure probability below a fixed value. The probabilistic approach of Rathje and Saygili (2008) and Saygili and Rathje (2009) is implemented by expressing the displacement as a function of ground motion parameters. Additionally, Kritikos *et al.* (2015) employed fuzzy logic to establish relationships between causative factors on landslide occurrence and, using the concept that the effect of some of them is similar in different regions, they estimated the relative probability of earthquake induced landslide occurrence at a given location.

The present study aims to contribute towards the evaluation of the earthquake-induced landslide hazard for the Greek region, which is characterized by a high level of seismicity and is among the most active regions globally. As a consequence, several cases of well documented landslides induced by historical and recent earthquakes exist (Papadopoulos and Plessa, 2000; Papathanassiou *et al.,* 2013). So far, however, no attempt has been made to assess this kind of hazard at regional scale by taking into account the characteristics of seismicity affecting Greece. In an effort to address this research gap, we provide the basis for the location of slopes exposed to significant probability of failures induced by future seismic events. Towards this goal, we apply the time probabilistic approach developed by Del Gaudio *et al.* (2003), with the aim of evaluating the strength demand required for slope stability under seismic shaking. Following this methodology, we present a thorough probabilistic seismic hazard assessment for different soil conditions in terms of Arias intensity expected, we produce regional maps representing the minimum resistance required for slopes to keep failure probability below a fixed value. These maps provide an important input for the evaluation of the exposure of Greece to seismic landsliding. The possible use of such maps in hazard estimates is finally exemplified through a direct comparison with actual critical acceleration values calculated for a coastal area of the Western Gulf of Corinth.

Methodology and input parameters

The implementation of the time probabilistic approach adopted in the present study first quantifies the expected level of seismic shaking in terms of Arias intensity calculated on the largest ground motion component ($I_α$); then the slope strength demand is represented through the slope critical acceleration (α_c) and the conditions for earthquake landslide triggering are derived from the estimated amount of Newmark's displacement (D_n). The use of the largest ground motion component of Arias intensity is justified by the fact that, for the assessment of seismically induced landslide hazard, one should use a shaking parameter representative of ground motion along a specific direction (i.e. the potential sliding direction) rather than the total shaking energy released in the horizontal plane. The lack of knowledge of actual shaking in such direction introduces a random error in the modeling of earthquake effects, which, however, can be statistically treated, whereas the use of the sum of the two horizontal components would tend to introduce a systematic overestimate. The methodology takes into consideration the characteristics of the seismicity affecting a given study area and ultimately estimates the critical acceleration $(A_c)_x(p,t)$ that slopes should have to limit within a prefixed threshold p the probability that, within a time t, Newmark's displacement will exceed a critical value x. The derived critical acceleration values are consequently representative of the slope strength demand of a given area in order to keep the future earthquake-induced slope failure probability below a fixed limit in the time interval considered.

The calculation of $(A_c)_x(p,t)$ values requires the preliminary choice of the probability parameters p and t, along with the critical threshold x of Newmark displacement. As far as the probability parameters are concerned, in the present study we adopt an exceedance probability of 10% in 50 yr, which is commonly adopted by building codes for seismic design purpose. Regarding the Newmark displacement thresholds, we consider the values of 2 cm and 10 cm that were suggested by Wilson and Keefer (1985) as critical thresholds for potential seismic triggering of incoherent (rock falls, disrupted slides, rock avalanches) and coherent (slumps, block slides, slow earth flows) landslides, that typically affect rock slopes and soil slopes, respectively.

Towards calculating *$(A_c)_x$*, the first step is to apply the Cornell (1968) method to obtain the occurrence probabilities for different levels of seismic shaking, expressed in terms of I_α, in a 50 year time interval at a grid of sites covering our study area. This computation was performed using the Crisis2007 code (Ordaz *et al.,* 2007). Such code requires as input elements i) a seismic source-zone model, ii) the rate of generation of different sized earthquakes in each of these zones and iii) a ground motion predictive equation. For the present investigation, we adopted the seismotectonic zonation developed within the framework of the SHARE Project along with the corresponding maximum magnitudes, prevailing faulting style and seismicity rate parameters including the a- and b-values of the Gutenberg-Richter frequency relationship (Giardini *et al.,* 2013). Figure 1 shows the seismogenic zonation and spatial distribution derived from the catalog of the National Observatory of Athens (NOA). As ground motion predictive equation (GMPE) for Arias intensity I_α we employed the following formulae obtained by Chousianitis *et al.* (2014):

$$log I_\alpha = -4.968 + 0.93M - 1.284 log\sqrt{R^2 + 6.282} - 0.006\sqrt{R^2 + 6.282} + 0.235m \pm 0.591 \quad (1)$$

for rock sites, and

$$log I_\alpha = -5.201 + 0.93M - 1.154 log\sqrt{R^2 + 5} - 0.007\sqrt{R^2 + 5} + 0.432 + 0.272m \pm 0.584 \quad (2)$$

for soil sites, where M is the moment magnitude, R is the epicentral distance and m represents the effect of the focal mechanism (equal to 1 for thrust/strike slip type and 0 for normal type). The coefficients of these equations were obtained from regressions using a data set or recordings acquired at distances from 1 to 195 km, for events of M_w between 4.1 and 6.6, which caused recorded Arias intensity values between 0.001 and 1.15 m/s. Thus, the use of equations (1) and (2) beyond these boundaries implies estimate uncertainties increasing as more one moves away from the regression limits. Since these predictive equations take into account the type of faulting, we assigned thrust and strike-slip mechanisms, to all the seismogenic sources belonging to the Hellenic Arc system and the North Anatolian Fault. Eventually, through discretization of the possible I_α value range into classes up to its maximum, this step provided the number of events expected to cause different values of I_α during 50 years at each node of the grid (see Fig. 2a).

Afterwards, we used the following empirical relation of Chousianitis *et al.* (2014) that links Newmark displacement to Arias intensity and to slope critical acceleration, i.e.

$$logD_n = 2.228logI_\alpha - 2.498log\alpha_c + 0.373logI_\alpha log\alpha_c - 5.495 \pm 0.237 \qquad (3)$$

where D_n is the Newmark Displacement, I_α is the Arias intensity and α_c is the critical acceleration. The coefficients of this equation were obtained from the regression of the results of accelerometer recording numerical integrations carried out fixing critical accelerations values between 0.02 and 0.2 g, thus its use beyond these limits implies uncertainties possibly larger than those quantified by the regression standard deviation. The expression (3) was used to derive the probability that observed D_n values exceed critical thresholds equal to 2 cm and 10 cm for discretized values of I_α and for fixed values of α_c. This was achieved by assuming a normal distribution of log D_n around the value predicted by the aforementioned empirical equation and integrating the probability curve from the threshold values of 2 cm or 10 cm to infinity (Fig. 2b). The calculation of D_n exceedance probabilities was carried out for each value of the I_α

classes defined earlier: the resulting values were multiplied by the number of events expected for each I_α class at each grid node and the results were summed to obtain the cumulative probability of exceedance of D_n (Fig. 2c). At each node of the grid, the D_n exceedance probabilities are iteratively calculated searching, through a bisection approach, couple of α_c values providing exceedance probability approximating by excess and by defect the target value (e.g., 10%). The range of the couple of α_c values is progressively restricted until a predefined level of approximation of the searched solution is reached: finally, the average of the final α_c range is assumed as $(A_c)_x$ value for the grid node.

That way we mapped the spatial distribution of minimum critical acceleration that slopes needs to have locally to keep within 10% the probability that Newmark's displacement will exceed 2 cm or 10 cm in 50 years, for rock and soil slopes, respectively. These maps represent the spatial distribution of the strength demand required for slopes to resist failure under the action of the regional seismicity for the case of incoherent and coherent landslides, respectively. Since these maps are calculated only on the basis of seismicity characteristics, they represent an alternative way to express the seismic potential of a region. At the same time they can be used as a reference for a direct comparison with actual critical acceleration in order to identify areas prone to seismically-induced failures and to define target of preventive slope stabilization measures (e.g., Del Gaudio and Wasowski, 2004; Rajabi *et al.,* 2013).

Slope strength demand computation

Before presenting the results of the time probabilistic evaluation of earthquake-induced landslide hazard for the Greek area, we will discuss the results of the Cornell method in terms of Arias intensity, which is considered a preliminary indicator of the capacity of the ground shaking caused by earthquakes to trigger landslides. Figure 3a and 3b depict the probabilistic Arias intensity predictions for a return period of 475 years and for the cases of rock and soil site conditions respectively. Additionally, Figure 4a and 4b show the probability that in 50 years Arias intensities will exceed 0.11 and 0.32 m/s, which correspond to critical thresholds for the triggering of incoherent and coherent landslides respectively. Since the former type of landslides typically affect rock slopes, while the second usually occurs in soil slopes, we use the GMPE for rock site conditions (equation 1) in the calculation of the values of Figure 4a, and that for soil site conditions (equation 2) in the calculation of the values of Figure 4b.

Inspecting Figure 3, we preliminarily note that Arias intensity values with exceedance probability of 10% in 50 years for soil sites are up to about twice as much as those for rock sites. This reflects the influence of the site terms in equation (2) which determines a relative amplification by an approximate factor of 2, affecting soil sites in comparison to rock sites. Comparing the values obtained for the two types of site conditions, with the thresholds proposed by Keefer and Wilson (1989) for landslide triggering, one can observe that, with the exception of the low seismic hazard area of central Aegean Sea, the threshold of 0.11 m/s is exceeded everywhere, implying that the whole Greek territory is at least at incoherent landslide risk. Also, it is clearly outlined that, regarding rock site conditions, the areas of Western Greece, Gulf of Corinth and Northern

Aegean, have a significant slope instability potential for all kinds of landslides due to the exceedance of the critical threshold of 0.54 m/s, while for soil site conditions, this threshold is exceeded in the majority of mainland Greece. Within the Greek territory, the largest Arias intensity values were found in coastal areas and islands of Ionian Sea and around the Gulf of Corinth, where values up to 2 m/s for rock site conditions and 3.5 m/s for soil type conditions were obtained.

The high potential for earthquake-induced landslide occurrence in the Ionian Sea area is also depicted on both maps of Figure 4. In this region, the exceedance probability in 50 years for the aforementioned thresholds reaches 90% in the case of 0.11 m/s for rock site conditions and 70% in the case of 0.32 m/s for soil site conditions. This area has a rich history of landslides induced by strong events and during the last 10 years two cases of diffuse landslide mobilization as effect of earthquakes occurred. The 2003 Lefkada earthquake ($M_w = 6.3$) triggered many landslide events, particularly rock falls, which occurred mainly at the western part of the Lefkada island (Papathanassiou *et al.,* 2013). Recently, two strong earthquakes that ruptured the western Cephalonia Island on January 26 and February 3, 2014 ($M_w = 6.0$ and $M_w = 5.9$ respectively), caused several rock falls on the western part of the island. Throughout continental Greece, probabilities of exceedance range from very low values up to values that reach 50% for both I_α thresholds, with the highest values obtained at the areas of central Greece and secondarily at Chalkidiki peninsula, and the lowest at western-central Macedonia and southeastern Peloponnese. It is noteworthy that, despite the higher values of Arias intensity expected for soil sites, the probability of exceedance of thresholds for incoherent landslides on rock slopes appears similar to, and even higher than for coherent landslides on soil slopes. This reflects the fact that the thresholds for coherent landslide triggering is almost three times as much as that for incoherent landslides, which decreases the threshold exceedance probability, compensating the relative amplification by a factor of 2 expected on soil slopes.

Maps like those of Figure 3 and Figure 4 give some preliminary indications of the areas potentially subject to conditions of slope instability under seismic actions, i.e. areas where high Arias intensity larger than critical thresholds are expected with high exceedance probabilities. However, this is a rather rough representation of earthquake-induced landslide hazard, in that these maps are calculated without taking into account the connection between the level of earthquake shaking and the co-seismic slope performance. This gap can be filled by transforming, through the procedure described in the previous section, hazard maps expressed in terms of a seismic shaking parameter into maps of strength demand represented by the values of $(A_c)_2$ (for rock sites) and $(A_c)_{10}$ (for soil sites), calculated for Newmark displacement exceedance probability of 10 % in 50 years.

The resulting values are shown in Figure 5. It can be preliminarily observed that the $(A_c)_2$ values are considerably higher than the $(A_c)_{10}$ values, reaching a maximum of 0.44 g in Cephalonia island, whereas in the same area $(A_c)_{10}$ does not exceed 0.17 g. This depends on the fact that the stronger ground motion expected on soil sites is overcompensated by the much higher value of the D_n critical threshold defining the limit of slope stability conditions. $(A_c)_2$ values larger than 0.2 g are found throughout Western Greece: at this regard, it should be reminded that the equation (3) does not provide reliable estimates of Newmark displacement for critical accelerations larger than 0.2 g, thus, in the areas where the calculation of $(A_c)_x$ gave larger values, these are to be considered with some caution. These areas, in terms of relative hazard, are certainly the most exposed to conditions of landslide seismic triggering, but the real strength demand for slopes to have a probability of 90% to resist to seismic failures in 50 years must be considered larger than 0.2 g and its exact definition would require specific studies.

Another area with a significantly high value of hazards is that around the Gulf of Corinth, where $(A_c)_2$ exceeds 0.1 g, whereas values larger than 0.08 g are found in central Greece and in eastern part of the Chalkidiki peninsula. With regard to $(A_c)_{10}$, values larger than 0.1 g are reached only in the Ionian islands and in the westernmost part of Greece mainland. For most of the remaining territory $(A_c)_{10}$ is less than 0.05 g. This value, according to Wilson and Keefer (1985), could be considered a minimum threshold to characterize slopes susceptible to seismic failure, in that lower values imply a level of instability that make more probable failures as effect of more frequent non-seismic events (e.g., heavy rainfalls). However a study conducted in southern Italy (Del Gaudio and Wasowski, 2004) showed that, possibly in dependence on local climatic conditions, it is possible that a large number of marginally stable slopes can survive non-seismic mobilising actions until an earthquake cause diffuse failures. Thus, any evaluation on the actual hazard requires an accurate estimate of the critical acceleration characterizing local slopes.

Comparison with in situ critical acceleration values

The spatial distribution of the $(A_c)_x$ values of Figure 5 can serve as input for a direct comparison with actual critical acceleration values purposely calculated at a more local scale in order to identify areas prone to earthquake-induced failures. As an example, we considered a region located in the western part of the Gulf of Corinth (inset of Fig. 6a). The Gulf of Corinth is one of the most active intra-continental tectonic rifts around the world and is characterized by the occurrence of several moderate to strong events as well as by significant background seismicity (e.g., Bernard *et al.,* 2006; Bourouis and Cornet, 2009; Lambotte *et al.,* 2014). The Corinth rift is a region of rapid extension and, as GPS studies have revealed, its western tip exhibits the highest extensional rates which reaches 15 mm/yr giving strain rate values up to 220 ns/yr (e.g., Avallone *et al.,* 2004; Chousianitis *et al.,* 2013; Chousianitis *et al.,* 2015). Onshore and offshore normal faults in the rift zone trend WNW-ESE with a maximum surface trace of about 25 km (Stefatos *et al.,* 2002; Moretti *et al.,* 2003). Uplift rates calculated for Quaternary terraces differ along the Corinth rift and range from 0.8-1 mm/yr near its western tip, to 0.3-0.4 mm/yr near the town of Corinth (Armijo *et al.,* 1996).

A large number of ground failure cases have occurred in the vicinity of Gulf of Corinth with a distribution which is consistent with the main WNW-ESE trend of the onshore and offshore normal faults of the rift zone (Koukis *et al.,* 2009). Heavy rainfall and/or earthquake activity constitute the main landslide triggering factors (Sabatakakis *et al.,* 2005). Analyzing seventy three (73) landslides located within the examined area, which were obtained from the existing landslide relational database management system (Sabatakakis *et al.,* 2013), some observations can be drawn: (a) the main types of landslides encountered (Varnes, 1984; Cruden and Varnes, 1996), include translational and rotational earth slides as well as earth and scree flows that involve 47% and 31% of the recorded occurrences respectively (Table 1); (b) the most critical landslide prone geological formations within the investigated area are the fine grained Neogene sediments/marls along with flysch, which is often highly sheared with 30% and 26% of the recorded occurrences respectively (Table 2).

The assessment of the exposure to landslide seismic induction using the parameter $(A_c)_x$ is a premise to hazard assessment based on its comparison with the actual critical acceleration values at each point of the investigated area. For this purpose, the first step is the evaluation of the static factor of safety. A limit-equilibrium model commonly used to represent slope failure conditions is the infinite slope model (Skempton and Delory, 1957), which assumes that mass movements occur along a sliding surface that extends infinitely down the slope. This model fits observations in the field in case of shallow landslides whose thickness is small in comparison to landslide length, and numerous authors (e.g., Jibson *et al.,* 2000; Saygili and Rathje, 2009; Dreyfus *et al.,* 2013) have relied on it to assess earthquake slope stability and calculate hazard maps of slope instability. Such a failure may take the form of a gradual downhill creep or may often involve a very sudden and extensive slide, while is closely related with instability phenomena encountered in the ground units of the studied area and especially in weathered flysch, shales-cherts and neogene sediments (Christoulas *et al.,* 1998; Sabatakakis *et al.,* 2005), as well as in recent deposits. Under these conditions, the static factor of safety, which is defined as the ratio of resisting forces to driving forces that cause failure, can be expressed as follows:

$$FS = \frac{c'}{\gamma_b Z \sin\alpha} + \frac{(1-r_u)\tan\varphi'}{\tan\alpha} \tag{4}$$

where c' is the effective cohesion, φ' is the effective angle of internal friction, γ_b is the material unit weight, Z is the failure's depth, α is the thrust angle and r_u is the pore pressure ratio (Bishop and Morgenstern, 1960). The thrust angle is the angle from the horizontal of the first movement of the center of mass of the potential landslide block and is typically approximated by the slope angle. The pore pressure ratio at a point below the ground surface is defined as:

$$r_u = \frac{u}{\gamma_b h} = \frac{\gamma_w Z_w}{\gamma_b Z} \quad (5)$$

where u is the pore pressure ($u = \gamma_w Z_w$), γ_w is the water unit weight (≈ 10 kN/m^3), Z_w is the height of table-water above the failure surface and $h = Z$ the considered point depth below the soil surface.

After the evaluation of the static factor of safety through equations (4) and (5), the next step in the Newmark model towards the calculation of critical acceleration, is the connection of the dynamic stability of a slope with its static stability and with geometry through the following relation:

$$\alpha_c = (FS - 1)\, g \sin \alpha \quad (6)$$

where α_c is the critical acceleration, FS is the static factor of safety of the slope, g is the acceleration due to gravity and α is the thrust angle of the landslide block.

To produce the critical acceleration map for the examined area, we implemented equations (4), (5) and (6) in a Geographical Information System (GIS). The GIS incorporates a powerful set of tools for the input, storage, retrieval, transformation and display of various data sets and have significantly improved our ability in calculating and managing natural hazards. Using the ArcGIS 9.3 software (ESRI, 2008) we created for each required input variable the corresponding digital thematic layer in raster format. First, in order to produce the static factor of safety map, the geotechnical parameters of all the geological units need to be calculated. A large number of engineering geological appraisals and geotechnical studies, conducted within the investigated area, provided valuable information about the engineering geological and geotechnical ground conditions. The majority of these studies utilized reliable data and samples from boreholes and trial pits that were drilled and excavated during the construction of public works such as motorways, railways and other large infrastructure projects. In addition, we collected and thoroughly analyzed data obtained by the Ministry of Environment as well as by private consultants. After the appropriate modifications to standardize the terminology, a large number of geotechnical profiles that characterize the local soil conditions were recorded and digitally stored. A relational geotechnical database management system was designed in MS Access to allow rapid retrieval and evaluation of the data in selected unit areas. The interplay between the database system and GIS was established by the coordinates of the locations of existing geotechnical profiles. Finally, a multipurpose large scale engineering geological map was compiled at a scale of 1:100,000 (Fig. 6a).

In the map of Figure 6a, the geological formations were grouped into 9 individual geotechnical units, on the basis of composition, physical state, relevant age, and engineering geological characteristics of the soil formations. Table 3 summarizes a description of each geotechnical unit along with representative input parameters for the proposed conceptual model of shallow translational slides on an infinite slope. The unified geotechnical parameters (effective shear strength and unit weight) for each unit were determined through a comprehensive evaluation of geotechnical data including: (a) The compilation of a large number of testing results on undisturbed soil samples obtained from the designed relational database management system; shear strength parameters in terms of effective stress that had been used for slope stability analyses, were retrieved to establish the value range and to estimate the mean representative values assuming a quite similar stress pattern in the field, (b) shear strength characteristics estimated from back analyses on specified slope failures with failure mechanism similar to the proposed infinite model especially in flysch (unit VII), marls (unit VI) and shales (unit IX), (c) rockmass classification systems (RMR and GSI) in heavily jointed and sheared rockmasses assuming isotropic behavior (units V and VIII), and (d) the experience gained over a long time period at technical works design and construction (road cuttings and slopes) in the ground units of the study area. The investigated area has a semi-wet to wet climate, with moderate water shortage in summer and humidity index from 0 to 40, while the mean annual precipitation ranges from 800 to 1000 mm. The natural groundwater conditions were specified using the pore pressure coefficient (r_u) which is the ratio of pore water pressure to the overburden pressure and generally represents the groundwater table fluctuation. The r_u values of the geotechnical units of the study area range from 0 to 0.4 (Table 3). The former value characterizes dry conditions for all ground members, while values above zero characterize wet conditions and generally range from 0.1-0.2 for permeable formations to 0.4 for less permeable cohesive and landslide prone members. Actually, the depth to the groundwater table will generally vary throughout the year and the worst conditions, when most failures take place, usually occur during intense rainfalls. In that case, the phreatic line at the surface of the slope is generally assumed. Additionally, we performed our calculations considering a failure depth equal to 5 m, which is a typical value for landslides in the examined region.

Subsequently, starting from a high accuracy (5x5 m) Digital Surface Model (DSM) provided by the Hellenic Military Geographical Service (HMGS), a slope map was generated (Fig. 6b) in GIS environment by applying an algorithm to compute the maximum slope of each cell from the comparison between the elevations of adjacent cells. The used high accuracy discretization contributes to "highlight" significant differences in slope inclination and ground geology that often exist between neighboring cells. The next step was to combine all the data layers relative to the parameters of equation (4) to estimate the static factor of safety and get a picture of its spatial distribution. Since the pore pressure coefficient is likely characterized by seasonal variation, we provided two maps of the static factor of safety according to the boundary values of r_u, that represent situations expected in dry and wet season (Fig. 6c), pointing out however the semi-wet to wet climate of the examined region. Areas of slope less than 10 degrees were not taken into account, considering negligible the landslide hazard in such conditions. Furthermore, in order to ensure the stability of the model before the earthquake shaking occurs, we modified the values of the static factor of safety below unity, following the approach of Dreyfus *et al.* (2013). The final static factor of safety maps had values ranging from just greater than 1, for steep slopes in weak and landslide prone ground material, to more than 5 in strong, permeable materials of gentle slopes.

Eventually, equation (6) was used to combine the GIS layers of the static factor of safety with the slope angle and compute the critical acceleration value for each pixel of the investigated area for conditions expected during a dry and a wet season (Fig. 6d). Subsequently, the real α_c values can be compared with the $(A_c)_x$ values obtained by the application of the time probabilistic approach. As demonstrated by the statistical analysis performed using the landslide occurrences located within the examined area, geological conditions for the triggering of coherent (slides and flows) landslides predominate. This is corroborated by the facts that only roughly 15% of the reported landsides are of incoherent type, and that the vast majority of the landslides have occurred on engineering soils and not on stiff rock slopes. Despite the larger frequency of coherent landsides within the examined area, with the aim of obtaining a comprehensive estimate of the earthquake-induced landslide hazard, we considered both types of landslides. We took into consideration which type affects the different geological units and for each of them we made the comparison with $(A_c)_2$ or $(A_c)_{10}$ accordingly. In this context, incoherent landslides have affected mainly the limestones, both types of landslides have occurred at flysch, marly conglomerates and the shales-sandstones-cherts of Figure 6a, while the rest geological formations have been affected only by coherent landslides. The locations where the actual α_c values were below the calculated $(A_c)_x$ values for the corresponding geological units indicated the slopes that have a significant probability of failing under seismic action in the future. Their spatial distribution for wet and dry conditions is shown in Figure 6e.

The zones of high susceptibility to seismic failures in both maps appear mainly at steep slopes consisting of shale and chert formations. This is confirmed by the results of Rozos *et al.* (2011) who acknowledge the large number of landslides there and explained it on the basis of the prevailing geological and morphological conditions. The rest of slopes which are characterized by high susceptibility were located at engineering soils. These results imply that for the examined area the hazard of seismically induced landslides is basically related to the possible triggering of coherent landslides, thus confirming the pre-existing observations within the examined area. One additional conclusion which can be drawn from the maps of Figure 6e is that the high susceptibility zones that are derived for the wet season cover a much larger area compared to those for the dry season. This way we demonstrated that the earthquake-induced landslide susceptibility mapping is dependent to a large degree by the natural groundwater conditions.

Discussion

The Newmark's sliding block model, which has been extensively applied to model the effects of a seismic event on natural slopes, is based on a series of assumptions, imposed for theoretical and practical simplicity, which limit the extent to which this model simulates the physical process. A first simplification derives from the physical characterization of the landslide as a rigid, perfectly plastic block resting on an inclined plane, which represents a potential failure surface, and subject, during earthquakes, to horizontal accelerations. Additional simplifications derive from the lack of consideration of three phenomena, i.e. : 1) the possible development of multiple slip surfaces (Wartman *et al.,* 2005); 2) the response of pore-pressure to shaking and 3) the shear strength loss as a function of strain after failure initiation (Wartman *et al.,* 2003; Wartman *et al.,* 2005).

The fundamental assumption is the rigid behavior of the sliding mass. While this constraint is appropriate for displacement analyses in the case of relatively thin sliding masses composed of stiff or brittle materials, it introduces modeling error for thicker landslides in softer slope-forming materials (Rathje and Bray, 1999; Wartman *et al.,* 2003). In this latter case, the rigid block assumption would be unconservative and for more realistic results the dynamic response of the sliding block needs to be considered, considering that site amplification phenomena increase slope susceptibility to seismic failures and promote the triggering of landslides (Havenith *et al.,* 2002; Del Gaudio and Wasowski, 2007; Moore *et al.,* 2011).

In response to these shortcomings, more rigorous methods have been developed, generally falling into the category of the flexible sliding block models. These include different kind of approaches: some of them, known as "decoupled" approaches, accounts for the dynamic response of the landslide material above a potential failure surface preliminarily to displacement calculation (Makdisi and Seed, 1978), others, defined as "coupled" approaches, model simultaneously the dynamic response of the sliding mass together with the effect of permanent displacement (Rathje and Bray, 1999). Both of these methods ignore the effect of block rotation that was proposed by Stamatopoulos (1996) and implemented by Baziar *et al.* (2012) in the modified decoupled analysis. A comprehensive presentation of the different methods is provided by Jibson (2011), who argues that each method is characterized by its own assumptions and epistemic uncertainties and their applicability depends on the studied conditions.

However, even though deep slope failures should be modeled as flexible sliding masses, it has been reported that the predominant mode of failure under seismic shaking for natural slopes is shallow sliding and thus, modeling by means of the rigid block approach is adequate for regional scales (Jibson, 2007; Saygili and Rathje, 2008; Pradel *et al.,* 2005).

With regard to other factors responsible of estimate uncertainties, the use of a purely horizontal input motion, can cause significant errors only when very steep slopes are analyzed. The presence of multiple slip surfaces generally cause an underestimate of actual displacement, but it has been demonstrated that as multiple shear surfaces develop with similar orientation in a localized area, the Newmark approach generally provide reasonable estimates of deformation (Wartman *et al.,* 2005). Also the neglect of dynamic pore-pressure response tend to cause displacement underestimates, but it can be justified for slopes consisting of impermeable materials such as compacted clays, shales and very dense sands.

In general, all the mentioned simplifications of the Newmark's model limit the accuracy of the obtained results in specific cases, however the Newmark's sliding-block model has been adopted for studies at regional scales because more sophisticated approaches demand the integration of a broad spectrum of high quality data, which are typically available only for local scale studies. This scale restriction applies as well to the evaluation of possible site amplification phenomena, which can be hardly assessed at regional scales, involving a combination of different factors mainly related to topography (Harp and Jibson, 2002; Meunier *et al.,* 2008; Del Gaudio and Wasowski, 2011) and to the physical characteristics of topsoil and subsoil layers (Bozzano *et al.,* 2008).

Considering these limitations, Newmark's displacement should be used in studies at regional scales not for a prediction of mass movement expected, but as an index correlated to slope performance (cf. Jibson *et al.,* 2000), expressing the closeness of slope to failure conditions. At this regard, a critical aspect of the method implementation is the reliability of Newmark's displacement threshold adopted to define such failure conditions. In the present study, we adopted the thresholds proposed by Wilson and Keefer (1985) on the basis of on their expert judgment and on analogies with building foundation behavior. These thresholds have been applied in many studies on the topic of earthquake-induced landslides and successive case studies have given support to their significance. For instance, Jibson et al. (2000), after having estimated Newmark's displacement for the scenario of the 1994 Northridge earthquake, found, from a comparison with a very detailed landslide inventory, a rapid increase of the percentage of landslide cells as the estimated Newmark's displacement increases from a few cm to 10 cm. Above this value the percentage levels off abruptly for displacement between 10 and 15 cm, which suggests a critical threshold for slope destabilization around the value proposed by Wilson and Keefer (1985) for coherent landslides.

A question of general interest raised from the application of time probabilistic approach of seismic landslide hazard to Greece, is the kind of use that one can make of the outcome of such an approach within hazard mitigation strategies. Actually, the parametric approach used in the present paper offers the possibility of "capturing" combinations of situations (shaking energy, slope angle, mechanical properties of slope material, water table level) that can imply a risk of slope destabilization in the scenario of future earthquakes, thus pointing out zones where landslides are more probable to occur in the future. In this context, maps like those of Figure 5 represent quantities correlated to failure probabilities, which, even only in relative terms, allow to focus the attention on zones that are most at risk of seismic failures, hence delimiting the areas where more advanced and site-specific investigations should be planned.

Since the $(A_c)_x$ values represent an alternative way to express the seismic potential of an area, they can be incorporated into landslide susceptibility analyses (LSA) as a causative factor layer representing the seismic information and utilized together with landslide inventories to build susceptibility models for the prediction of future landslides (e.g. Lee *et al.,* 2008). Maps like those of Figure 5, highlighting areas at risk of seismic landslides, can be used by decision makers into multi-criteria methods, such as the Analytical Hierarchy Process (AHP) and the Weighted Linear Combination (WLC), along with geological, geomorphological and socio-economic factors, to facilitate proper land-use suitability assessment (e.g., Bathrellos *et al.,* 2012; Bathrellos *et al.,* 2013; Papadopoulou-Vrynioti *et al.,* 2013; Youssef *et al.,* 2015). The $(A_c)_x$ values can be considered as reference values to obtain the required safety factors for engineering works and provide as well the basis to evaluate at a local scale whether specific slopes have significant probability of failing in the future.

We demonstrated the latter concept in the previous section where we made a comparison with actual critical acceleration values and delineated susceptibility zones. This kind of information can be used by local authorities to establish early warning systems and optimize the management of seismic-landslide hazard (e.g., Malet *et al.,* 2002; Noferini *et al.,* 2006; Drakatos *et al.,* 2013).

Conclusions

In the present study we focused on the probabilistic evaluation of earthquake-induced landslide hazard in Greece. Using Arias intensity to quantify the level of seismic shaking and through empirical relations based on the Newmark's model, we produced regional probabilistic hazard maps in terms of the strength demand required for slopes to resist failure under the action of the regional seismicity. We incorporated the characteristics of seismicity affecting Greece and calculated maps that depict the minimum critical acceleration values required for slopes to keep within 10% the probability that Newmark displacement exceeds the thresholds of 2 cm for incoherent landslides on rock slopes and 10 cm for coherent landslides on soil slopes in a time interval of 50 yr. The obtained results represent an alternative way to measure the expected seismic shaking with a certain exceedance probability and provide for the first time in Greece the necessary quantitative information towards a comprehensive evaluation of earthquake-induced landslide hazard at more local scales.

The adopted methodology initially facilitated a preliminary rough representation of earthquake-induced landslide hazard through a standard hazard estimate procedure in terms of Arias intensity. The highest potential of earthquake-induced landslide occurrence was found at the islands and the coastal areas of central Ionian Sea. This region comprises the most seismically active part of Greece and it has been affected by coseismic landsliding many times in the past. Regarding mainland Greece, the highest Arias intensity probabilities of exceedance were obtained for the areas of central Greece and, secondarily, of Chalkidiki peninsula, while the lowest probabilities were found at western-central Macedonia and southeastern Peloponnese. Next, we incorporated in our calculations the linkage between the level of seismic shaking and its effects on slope stability and we produced maps of $(A_c)_2$ and $(A_c)_{10}$ evaluated for rock sites and soil sites respectively. As it is expected, larger critical acceleration thresholds were obtained at more seismically active regions where the strength demand for a slope not to fail is higher. Additionally, it is apparent that the $(A_c)_2$ values are considerably higher than the $(A_c)_{10}$ values, a fact that is due to the overcompensation of the stronger ground motion expected on soil sites by the much higher value of the D_n critical threshold defining the limit of slope stability conditions.

Subsequently, as an example of moving from the large scale mapping of $(A_c)_x$ to a more local representation of the spatial hazard of earthquake-induced landslides, we considered a region located at the western part of the Gulf of Corinth. We used the potential of GIS to create various layers of information consisting of shear-strength, lithology and slope data. We determined the actual critical acceleration values of this region from the static factor of safety and from the slope geometry and finally we performed a direct comparison with the critical acceleration values obtained by the application of the time probabilistic approach. In this way we were able to locate slope areas where real critical acceleration values are below the strength demand and, consequently, the probability of seismic-landslide triggering is significantly higher. The derived maps which delineate the most susceptible areas to earthquake-induced slope instabilities were obtained for two extreme cases of the natural groundwater conditions. The results gave evidence that slope failure scenario differentiates at different seasons and therefore, seismic effects on slope stability depend to a large degree on the season of earthquake occurrence.

The regional maps of slope resistance demand calculated within the framework of the present study provide the basis to assess the sites that, according to the Newmark model, can potentially undergo shakings capable of inducing activation of slope failures in the time interval considered. Moving towards local scales by employing the described procedure for estimating real critical acceleration values, one can evaluate whether specific slopes have a significant probability of failing in the future.

Data and Resources

The seismotectonic zonation along with the corresponding seismicity parameters of each source zone necessary for the hazard computation are publically available at http://www.share-eu.org (last accessed May 2015). The GMT mapping software (Wessel and Smith, 1998) was used for the preparation of some figures in this paper.

References

Arias, A. (1970). A measure of earthquake intensity, in *Seismic Design for Nuclear Power Plants*, R. J. Hansen (Editor), MIT Press, Cambridge, Massachusetts, 438-483.

Armijo, R., B. Meyer, G. C. P. King, A. Rigo, and D. Papanastassiou (1996). Quaternary evolution of the Corinth Rift and its implications for the Late Cenozoic evolution of the Aegean, *Geophys. J. Int.* **126**, 11-53.

Avallone, A., P. Briole, A. M. Agatza-Balodimou, H. Billiris, O. Charade, C. Mitsakaki, A. Nercessian, K. Papazissi, D. Paradissis, and G. Veis (2004). Analysis of eleven years of deformation measured by GPS in the Corinth Rift Laboratory area, *Comptes Rendus-Geosci.* **336**, no. 4-5, 301-311.

Bathrellos, G.D., K. Gaki-Papanastassiou, H. D. Skilodimou, D. Papanastassiou, and K. G. Chousianitis (2012). Potential suitability for urban planning and industry development by using natural hazard maps and geological-geomorphological parameters, *Environ. Earth Sci.* **66**, no. 2, 537-548.

Bathrellos, G. D., K. Gaki-Papanastassiou, H. D. Skilodimou, G. A. Skianis, and K. G. Chousianitis (2013). Assessment of rural community and agricultural development using geomorphological-geological factors and GIS in the Trikala prefecture (Central Greece), *Stoch. Environ. Res. Risk Assess.* **27**, no. 2, 573-588.

Baziar, M.H., H. Rezaeipour, and Y. Jafarian (2012). Decoupled solution for seismic permanent displacement of earth slopes using deformation-dependent yield acceleration, *J. Earthquake Eng.* **16,** no. 1, 917-936

Bernard, P., H. Lyon-Caen, P. Briole, A. Deschamps, F. Boudin, K. Makropoulos, P. Papadimitriou, F. Lemeille, G. Patau, H. Billiris, et al. (2006). Seismicity, deformation and seismic hazard in the western rift of Corinth: new insights from the Corinth rift laboratory (CRL), *Tectonophysics* **426***,* 7-30.

Bishop, A. W., and N. R. Morgenstern (1960). Stability coefficients for earth slopes, *Geotechnique* **10**, no. 4, 23-32.

Bourouis, S., and F. H. Cornet (2009). Microseismic activity and fluid fault interactions: some results from the Corinth Rift Laboratory (CRL), Greece, *Geophys. J. Int.* **178**, no. 1, 561-580, doi: 10.1111/j.1365-246X.2009.04148.x.

Bozzano, F., L. Lenti, M. Martino, A. Paciello, and G. Scarascia Mugnozza (2008). Self-excitation process due to local seismicamplification responsible for the reactivation of the Salcito landslide (Italy) on 31 October 2002, *J. Geophys. Res.* **113**, B10312, doi:10.1029/2007JB005309.

Chousianitis, K., A. Ganas, and M. Gianniou (2013). Kinematic interpretation of present-day crustal deformation in central Greece from continuous GPS measurements, *J. Geodyn.* **71***,* 1-13.

Chousianitis, K., V. Del Gaudio, I. Kalogeras, and A. Ganas (2014). Predictive model of Arias intensity and Newmark displacement for regional scale evaluation of earthquake-induced landslide hazard in Greece, *Soil Dyn. Earthquake Eng.* **65**, 11-29.

Chousianitis, K., A. Ganas, and C.P. Evangelidis (2015). Strain and rotation rate patterns of mainland Greece from continuous GPS data and comparison between seismic and geodetic moment release, *J. Geophys. Res.* **120**, 3909-3931, doi: 10.1002/2014JB011762.

Christoulas, S., N. Kalteziotis, E. Gassios, N. Sabatakakis, and G. Tsiambaos (1988). Instability phenomena in weathered flysch in Greece, in *Proceedings of the 5th international symposium on landslides*, Lausanne. Balkema, Rotterdam, 103-108.

Cornell, C. A. (1968). Engineering seismic risk analysis, *Bull. Seismol. Soc. Am.* **58***,* 1583-1606.

Cruden, D. M., and D. J. Varnes (1996). Landslides Types and Processes, in *Landslides: Investigation and Mitigation*, A. K. Turner and R. L. Schuster (Editors), Transportation Research Board Special Report 247, National Academy Press, WA, 36-75.

Del Gaudio, V., P. Pierri, and J. Wasowski (2003). An approach to time-probabilistic evaluation of seismically induced landslide hazard, *Bull. Seismol. Soc. Am.* **93***,* 557-569.

Del Gaudio, V., and J. Wasowski (2004). Time probabilistic evaluation of seismically-induced landslide hazard in Irpinia (Southern Italy), *Soil Dyn. Earthquake Eng.* **24**, 915-928.

Del Gaudio, V., and J. Wasowski (2007). Directivity of slope dynamic response to seismic shaking, *Geophys. Res. Lett.* **34**, L12301, doi:10.1029/GL029842.

Del Gaudio, V., and J. Wasowski (2011). Advances and problems in understanding the seismic response of potentially unstable slopes, *Eng. Geol.* **122**, 73-83.

Drakatos, G., D. Paradissis, D. Anastasiou, P. Elias, A. Marinou, K. Chousianitis, X. Papanikolaou, E. Zacharis, P. Argyrakis, K. Papazissi, and K. Makropoulos (2013). Joint approach using satellite techniques for slope instability detection and monitoring, *Int. J. Remote Sens.* **34**, no. 6, 1879-1892, doi: 10.1080/2150704X.2012.731089.

Dreyfus, D., E. M. Rathje, and R. W. Jibson (2013). The influence of different simplified sliding-block models and input parameters on regional predictions of seismic landslides triggered by the Northridge earthquake, *Eng. Geol.* **163**, 41-54.

ESRI, (2008). ArcDoc for ArcGIS, version 9.3 Help on CDROM.

Giardini, D., J. Woessner, L. Danciu, H. Crowley, F. Cotton, G. Grünthal, R. Pinho, G. Valensise, S. Akkar, R. Arvidsson, et al. (2013). Seismic Hazard Harmonization in Europe (SHARE): Online Data Resource, doi: 10.12686/SED-00000001-SHARE.

Grünthal, G., and R. Wahlström (2012). The European‐Mediterranean Earthquake Catalogue (EMEC) for the last millennium, *J. Seismol.* **16**, no. 3, 535-557, doi: 10.1007/s10950-012-9302-y.

Harp, E. L., and R. C. Wilson (1995). Shaking intensity thresholds for rock falls and slides: Evidence from 1987 Whittier Narrows and Superstition Hills earthquake strong motion records, *Bull. Seismol. Soc. Am.* **85**, no. 6, 1739-1757.

Harp, E. L., and R. W. Jibson (2002). Anomalous concentrations of seismically triggered rock falls in Paicoma Canyon: are they caused by highly susceptible slopes or local amplification of seismic shaking?, *Bull. Seismol. Soc. Am.* **92**, no. 8, 3180-3189.

Havenith, H. B., D. Jongmans, E. Faccioli, K. Abdrakhmatov, and P.-Y. Bard (2002). Site effect analysis around the seismically induced Ananevo rockslide, Kyrgyzstan, *Bull. Seismol. Soc. Am.* **92**, 3190-3209.

Jibson, R. W., E. L. Harp, and J. A. Michael (2000). A method for producing digital probabilistic seismic landslide hazard maps, *Eng. Geol.* **58**, 271-289.

Jibson, R. W. (2007). Regression models for estimating coseismic landslide displacement, *Eng. Geol.* **91**, 209-218.

Jibson, R. W. (2011). Methods for assessing the stability of slopes during earthquakes – a retrospective, *Eng. Geol.* **122**, 43-50.

Keefer, D. K. (1984). Landslides caused by earthquakes, *Bull. Geol. Soc. Am.* **95**, 406-421.

Keefer, D. K., and R. C. Wilson (1989). Predicting Earthquake induced landslides with emphasis on arid or semi-arid environments, in *Landslides in a Semi-Arid Environment*, Inland Geological Society, P. M. Sadler and D. M. Morton (Editors), Vol. 2, 118-149.

Kokkalas, S., and I. K. Koukouvelas (2005). Fault-scarp degradation modeling in central Greece: the Kaparelli and Eliki faults (Gulf of Corinth) as a case study, *J. Geodyn.* **40**, 200-215.

Koukis, G., N. Sabatakakis, M. Ferentinou, S. Lainas, X. Alexiadou, and A. Panagopoulos (2009). Landslide phenomena related to major fault tectonics: rift zone of Corinth Gulf, Greece, *Bull. Eng. Geol. Environ.* **68**, 215-229.

Kritikos, T., T. R. Robinson, and T. R. H. Davies (2015). Regional coseismic landslide hazard assessment without historical landslide inventories: A new approach, *J. Geophys. Res.* **120**, 711-729, doi: 10.1002/2014JF003224.

Lambotte, S., H. Lyon-Caen, P. Bernard, A. Deschamps, G. Patau, A. Nercessian, F. Pacchiani, S. Bourouis, M. Drilleau, and P. Adamova (2014). Reassessment of the rifting process in the Western Corinth Rift from relocated seismicity, *Geophys. J. Int.* **197**, 1822-1844, doi: 10.1093/gji/ggu096.

Lee, C.-T., C.-C. Huang, J.-F. Lee, K.-L. Pan, M.-L. Lin, and J.-J. Dong (2008). Statistical approach to earthquake-induced landslide susceptibility, *Eng. Geol.* **100***,* 43-58.

Makdisi, F. I., and H. B. Seed (1978). Simplified procedure for estimating dam and embankment earthquake-induced deformations, *J. Geotech. Eng. Div. ASCE* **104**, 849-867.

Malet, J.-P., O. Maquaire, and E. Calais (2002). The Use of Global Positioning System Techniques for the Continuous Monitoring of Landslides - Application to the Super-Sauze Earth Flow (Alpes De Haute-Provence, France), *Geomorphology* **43***,* 33-54.

Meunier, P., N. Hovius, and J. A. Haines (2008). Topographic site effects and the location of earthquake induced landslides, *Earth Planet. Sci. Lett.* **275**, 221-232.

Moore, J. R., V. Gischig, J. Burjanek, S. Loew, and D. Fah (2011). Site Effects in Unstable Rock Slopes: Dynamic Behavior of the Randa Instability (Switzerland), *Bull. Seismol. Soc. Am.* **101**, 3110-3116.

Moretti, I., D. Sakellariou, V. Lykousis, and L. Micarelli (2003). The Gulf of Corinth: an active half graben?, *J. Geodyn.* **36***,* 323-340.

Newmark, N. M. (1965). Effects of earthquakes on dams and embankments, *Geotechnique* **15***,* 139-159.

Noferini, L., M. Pieraccini, D. Mecatti, G. Macaluso, G. Luzi, and C. Atzeni (2006). Long Term Landslide Monitoring by Ground-Based Synthetic Aperture Radar Interferometer, *Int. J. Remote Sens.* **27**, 1893-1905.

Ordaz, M., A. Aguilar, and J. Arboleda (2007). CRISIS2007: Program for computing seismic hazard, v. 5.1. Instituto de Ingenieria, UNAM, Mexico.

Papadopoulos, G.A., and A. Plessa (2000). Magnitude-distance relations for earthquake-induced landslides in Greece, *Eng. Geol.* **58**, 377-386.

Papadopoulou-Vrynioti, K., G. D. Bathrellos, H. D. Skilodimou, G. Kaviris, and K. Makropoulos (2013). Karst collapse susceptibility mapping considering peak ground acceleration in a rapidly growing urban area, *Eng. Geol.* **158**, 77-88.

Papathanassiou, G., I. Valkaniotis, A. Ganas, and S. Pavlides (2013). GIS-based statistical analysis of the spatial distribution of earthquake-induced landslides in the island of Lefkada, Ionian Islands, Greece, *Landslides* **10**, 771-783, doi: 10.1007/s10346-012-0357-1.

Pradel, D., P. M. Smith, J. P. Stewart, and G. Raad (2005). Case history of landslide movement during the Northridge earthquake. *J. Geotech. Geoenviron. Eng. ASCE* **131**, 1360-1369.

Rajabi, A., M. Khamehchiyan, M. R. Mahdavifar, V. Del Gaudio, and D. Capolongo (2013). A time probabilistic approach to seismic landslide hazard estimates in Iran, *Soil Dyn. Earthquake Eng.* **48***,* 25-34.

Rathje, E. M., and J. D. Bray (1999). An examination of simplified earthquake-induced displacement procedures for earth structures. *Canadian Geotech. J.* **36**, 72-87.

Rathje, E. M., and G. Saygili (2008). Probabilistic seismic hazard analysis for the sliding displacement of slopes-Scalar and vector approaches, *J. Geotech. Geoenviron. Eng. ASCE* **134***,* 804-814.

Rodriguez, C.E., J. J. Bommer, and R. J. Chandler (1999). Earthquake-induced landslides: 1980–1997, *Soil Dyn. Earthquake Eng.* **18***,* 325-346, doi: 10.1016/S0267-7261(99)00012-3.

Rozos, D., G. D. Bathrellos, and H. D. Skilodimou (2011). Comparison of the implementation of Rock Engineering System (RES) and Analytic Hierarchy Process (AHP) methods, based on landslide susceptibility maps, compiled in GIS environment. A case study from the Eastern Achaia County of Peloponnesus, Greece, *Environ. Earth Sci.* **63**, no. 1, 49-63.

Sabatakakis, N., G. Koukis, and D. Mourtas (2005). Composite landslides induced by heavy rainfalls in suburban areas: city of Patras and surrounding area, western Greece, *Landslides* **3***,* 202-211.

Sabatakakis, N., G. Koukis, E. Vassiliades, and S. Lainas (2013). Landslide susceptibility zonation in Greece, *Nat. Hazards* **65**, no. 1, 523-543. doi: 10.1007/s11069-012-0381-4.

Saygili, G., and E. Rathje (2008). Empirical predictive models for earthquake-induced sliding displacements of slopes, *J. Geotech. Geoenviron. Eng. ASCE*, **134**, no. 6, 790-803.

Saygili, G., and E. M. Rathje (2009). Probabilistically based seismic landslide hazard maps: an application in Southern California, *Eng. Geol.* **109***,* 183-194.

Skempton, A.W., and F. A. Delory (1957). Stability of Natural Slopes in London Clays, in *Proceedings of the 4th International Conference on Soil Mechanics and Foundation Engineering,* **2***,* 378-381.

Stamatopoulos, C. A. (1996). Sliding system predicting large permanent co-seismic movements of slopes, *Earthquake Eng. Struct. Dyn.* **25**, no. 10, 1075-1093.

Stefatos, A., G. Papatheodorou, G. Ferentinos, M. Leeder, and R. Collier (2002). Seismic reflection imaging of active offshore faults in the Gulf of Corinth: their seismotectonic significance, *Basin Res.* **14***,* 487-502.

Stucchi, M., A. Rovida, A. A. Gomez Capera, P. Alexandre, T. Camelbeeck, M. B. Demircioglu, V. Kouskouna, P. Gasperini, R. M. W. Musson, M. Radulian, et al.

(2012). The SHARE European Earthquake Catalogue (SHEEC) 1000–1899, *J. Seismol.* **17**, no. 2, 523-544, doi: 10.1007/s10950-012-9335-2.

Varnes, D. J., and IAEG Commission on Landslides (1984). Landslides Hazard Zonation: a review of principles and practice, UNESCO, Paris, 63 pp.

Wartman, J., J. D. Bray, and R. B. Seed (2003). Inclined plane studies of the Newmark sliding block procedure, *J. Geotech. Geoenviron. Eng. ASCE* **129**, 673-684.

Wartman, J., R. B. Seed, and J. D. Bray (2005). Shaking table modeling of seismically induced deformations in slopes, *J. Geotech. Geoenviron. Eng. ASCE* **131**, 610-622.

Wessel, P., and W.H.F. Smith (1998). New, improved version of Generic Mapping Tools released, *Eos Trans. AGU* **79**, 579.

Wilson, R. C., and D. K. Keefer (1985). Predicting the areal limits of earthquake-induced landsliding, in *Evaluating Earthquake Hazards in the Los Angeles region - An Earth Science Perspective*, J. I. Ziony (Editor), U.S. Geol. Surv. Profess. Pap. 1360, 316-345.

Youssef, A. M., B. Pradhan, M. Al-Kathery, G. D. Bathrellos, and H. D. Skilodimou (2015). Assessment of rockfall hazard at Al-Noor Mountain, Makkah city (Saudi Arabia) using spatio-temporal remote sensing data and field investigations, *J. Afr. Earth Sci.* **101**, 309-321.

Full mailing addresses for each author

Institute of Geodynamics, National Observatory of Athens, Lofos Nymfon, 11810 Athens, Greece

K. Chousianitis: chousianitis@noa.gr

G. Drakatos: g.drakat@noa.gr

Dipartimento di Scienze della Terra e Geoambientali, Università degli Studi di Bari, via E. Orabona 4, 70125, Bari, Italy

V. Del Gaudio: vincenzo.delgaudio@uniba.it

Laboratory of Engineering Geology, Department of Geology, University of Patras, 26500, Patras, Greece

N. Sabatakakis: sabatak@upatras.gr

K. Kavoura: kavoura@upatras.gr

Department of Geography, Faculty of Geology and Geoenvironment, National and Kapodistrian University of Athens, University Campus, 15784, Zografou, Athens, Greece

G. Bathrellos: gbathrellos@geol.uoa.gr

H. Skilodimou: hskilodimou@geol.uoa.gr

Tables

Table 1. Frequency of the recorded landslide occurrences according to the type of movement.

Type of movement		Type of material	
		Bedrock	Engineering soils
Fall		16	
Topple		-	
Slide	Rotational		22
	Translational	-	25
Spread			-
Flow			31
Complex			6

Table 2. Frequency of the recorded landslide occurrences according to the lithology of the displaced material.

Lithology	Landslide occurrences	Landslide frequency LF (%)
Recent loose coarse grained deposits	2	3
Dilluvial coarse grained formations	8	11
Dilluvial formations of mixed phases	4	5
Conglomerates	11	15
Clayey marls	22	30
Flysch	19	26
Limestones	7	10

Table 3. Geotechnical parameters assigned to the engineering geological - geotechnical units of the investigated area.

	Unit	Description	c' (kPa)	Φ' (°)	γ_b (kNt/m^3)	r_u
I	Recent loose coarse grained deposits	River terrace deposits of sandy gravels (GM, GP-GM, GW-GM, GC) with cobles and silty sands (SM, SM-SC)	50	25	18.5	0-0.1
II	Recent loose deposits of mixed phases	Recent alluvial deposits of brown to brownish-gray silty clays (CL, CH) and silts (ML, ML-CL) with intercalations of silty sands (SM, SM-SC)	60	22	19.0	0-0.2
III	Diluvial coarse grained formations	Old alluvial-diluvial formations of brown to brownish-red dense sandy and clayey gravels (GW-GM, GC) with cobles- loose conglomerates	70	28	19.0	0-0.1
IV	Diluvial formations of mixed phases	Old alluvial-diluvial formations of brownish-red to brownish-grey silts, sandy silts sandy clays and silts (CL, CH, ML), with intercalations of sands, clayey-silty sands, silty sands and clayey gravels (GW-GM, GC, SM)	75	25	19.5	0-0.2
V	Marly conglomerates	Pleistocene very loose to weak conglomerates with sub-rounded to rounded gravels and pebbles (of limestone, sandstone and chert origin) cemented with clayey – marly matrix	150	32	25.0	0-0.1
VI	Clayey marls	Plio-Pleistocene, fluvial – fluviolacustrine sediments including a lower horizon of black – gray stiff silty marls	70	28	21.0	0-0.4

		and sandy silts (CL,CH, CL–ML, ML, SM) and an upper one of brownish – yellow stiff clayey marls with silts and sands (CL, ML, SM)				
VII	Flysch	Layers of shales, marls, siltstones and sandstones. Rockmass highly disintegrated and sheared with a weathered zone of several meters thick	60	25	23.0	0-0.4
VIII	Limestones	Cretaceous thin bedded limestones with cherts. Rockmass blocky-disturbed	200	30	26.0	0-0.1
IX	Shales - Sandstones-Cherts	Shale, sandstones and cherts. Rockmass highly disintegrated and sheared	55	25	23.0	0-0.4

Figure captions

Figure 1. Seismicity map showing shallow earthquakes with M_w>4.0. Epicenters are taken from the SHARE European Earthquake catalog (Grünthal *et al.,* 2012; Stucchi *et al.,* 2012). Superimposed are the SHARE seismogenic source zones.

Figure 2. Outline of the procedure for the evaluation of $(A_c)_x$. First (a), the number of events expected to cause different values of I_α at a given site are calculated. Then (b), for fixed values of critical acceleration α_c and for any I_α value, an empirical formula relating D_n to I_α and α_c is used to calculate the median expected values of D_n (dashed vertical line): assuming for its actual values a log-normal probability distribution, the probability is calculated that D_n exceeds a critical threshold (e.g., 10 cm) by integrating the probability curve from the D_n threshold to infinity (shaded area). The outcome of steps a) and b) are multiplied to obtain (c) the cumulative probability that D_n exceeds a critical threshold taking into account all the possible I_α values: calculations are iterated for different values of α_c, searching, through a bisection approach, the values that makes the D_n exceedance probability equal to a target value (e.g., 10% in 50 years). Note that the numbering of trial α_c values indicates the sequence of the trial in the solution search.

Figure 3. Arias intensity values with 90% probability of not being exceeded in 50 years (475 years return period) for (a) rock and (b) soil site conditions.

Figure 4. Probabilities of exceedance in 50 years of Arias intensity thresholds equal to (a) 0.11 for rock site conditions and (b) 0.32 m/s for soil type conditions.

Figure 5. Strength demand, expressed by critical acceleration $(A_c)_x$, requested to slopes in order to keep within 10% the probability of the occurrence of events causing, in a time span of 50 years, the exceedance of Newmark's displacement thresholds x equal to (a) 2 cm on rock slopes and (b) 10 cm in soil slopes.

Figure 6. (a) Simplified engineering geological map with major faults (after Kokkalas and Koukouvelas, 2005) of the study area (marked by the thick-line rectangle in the inset box). (b) Slope map created from Digital Surface Model. (c) Static factor of safety maps produced by applying equation (4) to raster data layers for situations expected in dry (left) and wet season (right) as discussed in text. (d) Distribution of the critical acceleration values obtained from combining the static factor of safety layer with the slope angle layer according to equation (6) for dry (left) and wet (right) season. (e) Map showing the locations where the actual α_c values are below the calculated $(A_c)_\chi$ values, indicating the slopes that have a significant probability of failing under seismic action in the future for dry (left) and wet (right) season.

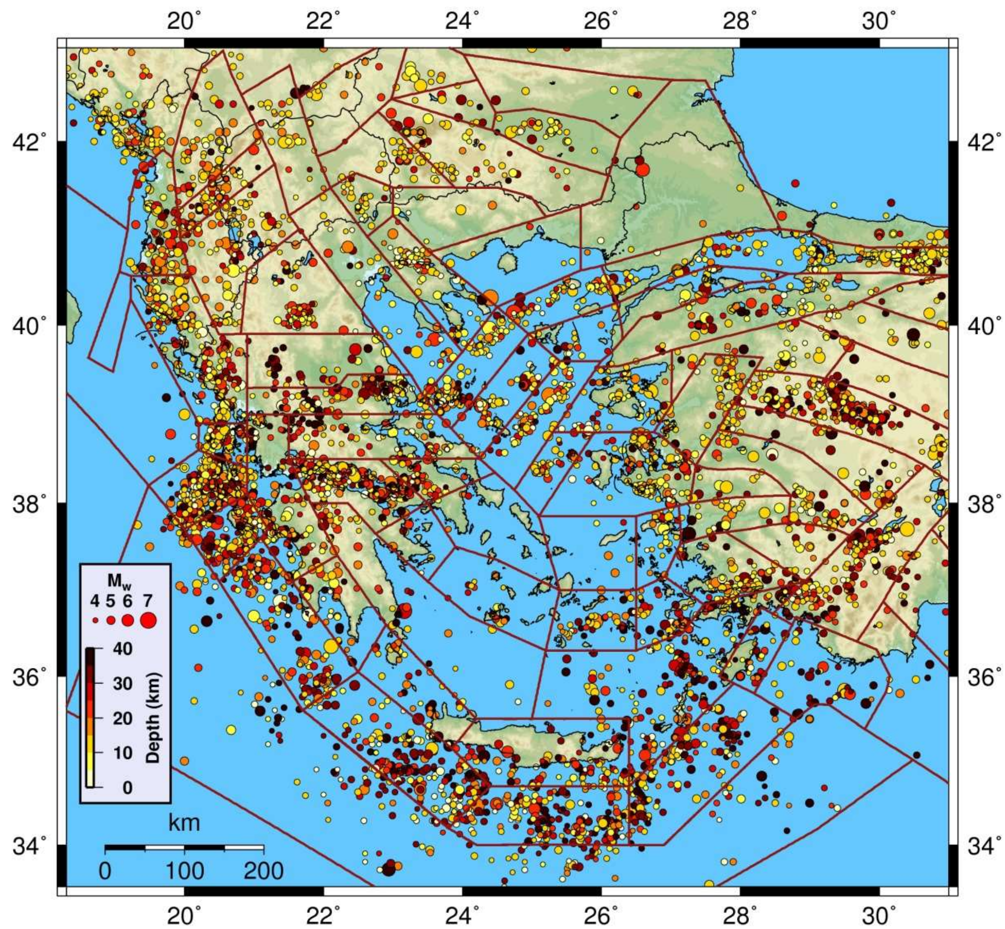

Figure 1. Seismicity map showing shallow earthquakes with M_w>4.0. Epicenters are taken from the SHARE European Earthquake catalog (Grünthal *et al.,* 2012; Stucchi *et al.,* 2012). Superimposed are the SHARE seismogenic source zones.

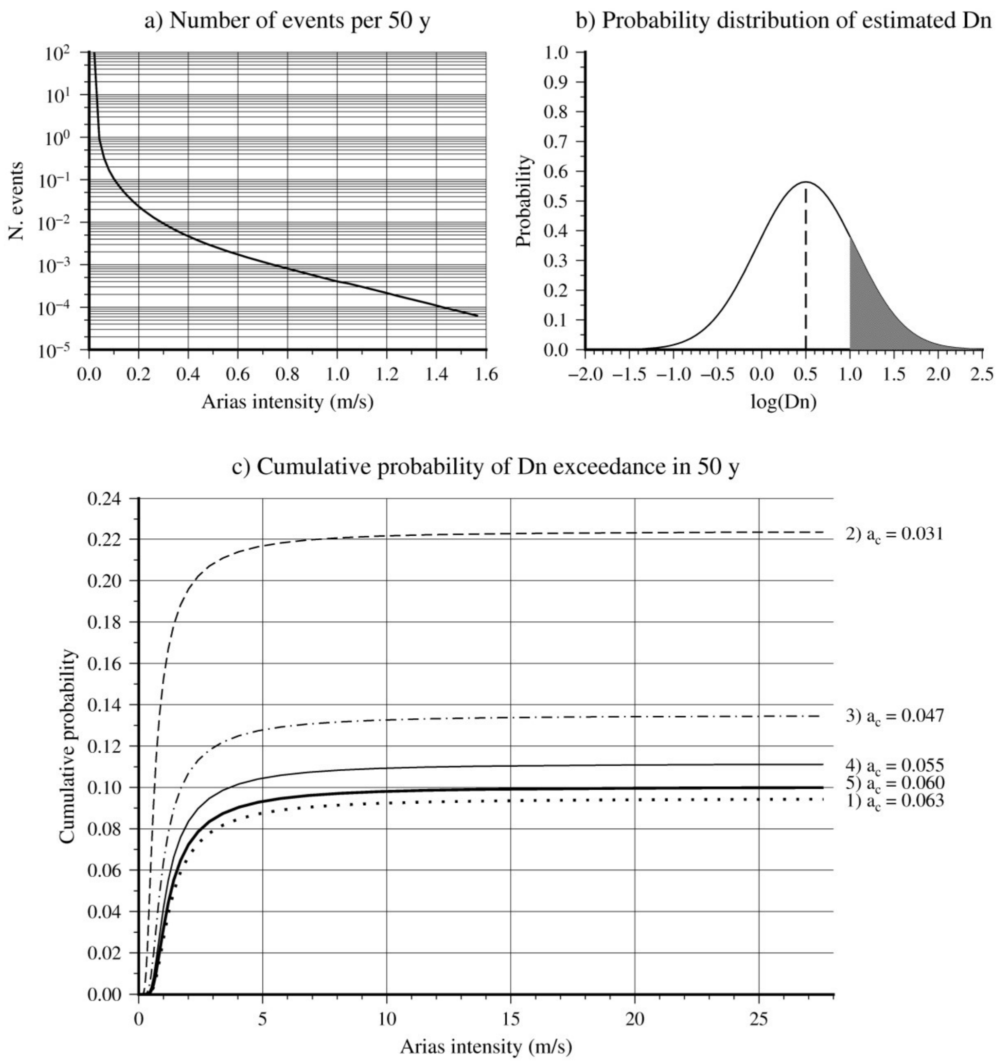

Figure 2. Outline of the procedure for the evaluation of $(A_c)_x$. First (a), the number of events expected to cause different values of I_α at a given site are calculated. Then (b), for fixed values of critical acceleration α_c and for any I_α value, an empirical formula relating D_n to I_α and α_c is used to calculate the median expected values of D_n (dashed vertical line): assuming for its actual values a log-normal probability distribution, the probability is calculated that D_n exceeds a critical threshold (e.g., 10 cm) by integrating the probability curve from the D_n threshold to infinity (shaded area). The outcome of steps a) and b) are multiplied to obtain (c) the cumulative probability that D_n exceeds a

critical threshold taking into account all the possible I_α values: calculations are iterated for different values of α_c, searching, through a bisection approach, the values that makes the D_n exceedance probability equal to a target value (e.g., 10% in 50 years). Note that the numbering of trial α_c values indicates the sequence of the trial in the solution search.

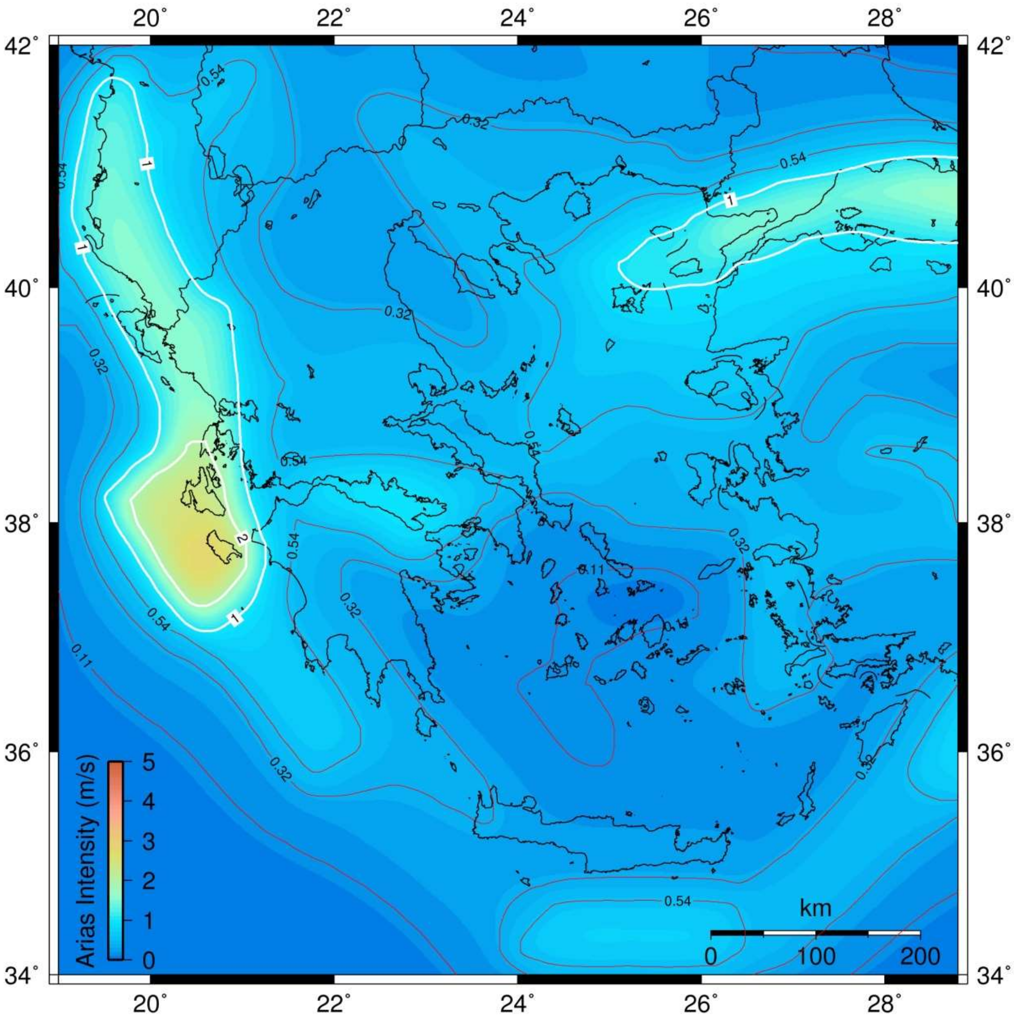

Figure 3a. Arias intensity values with 90% probability of not being exceeded in 50 years (475 years return period) for (a) rock conditions.

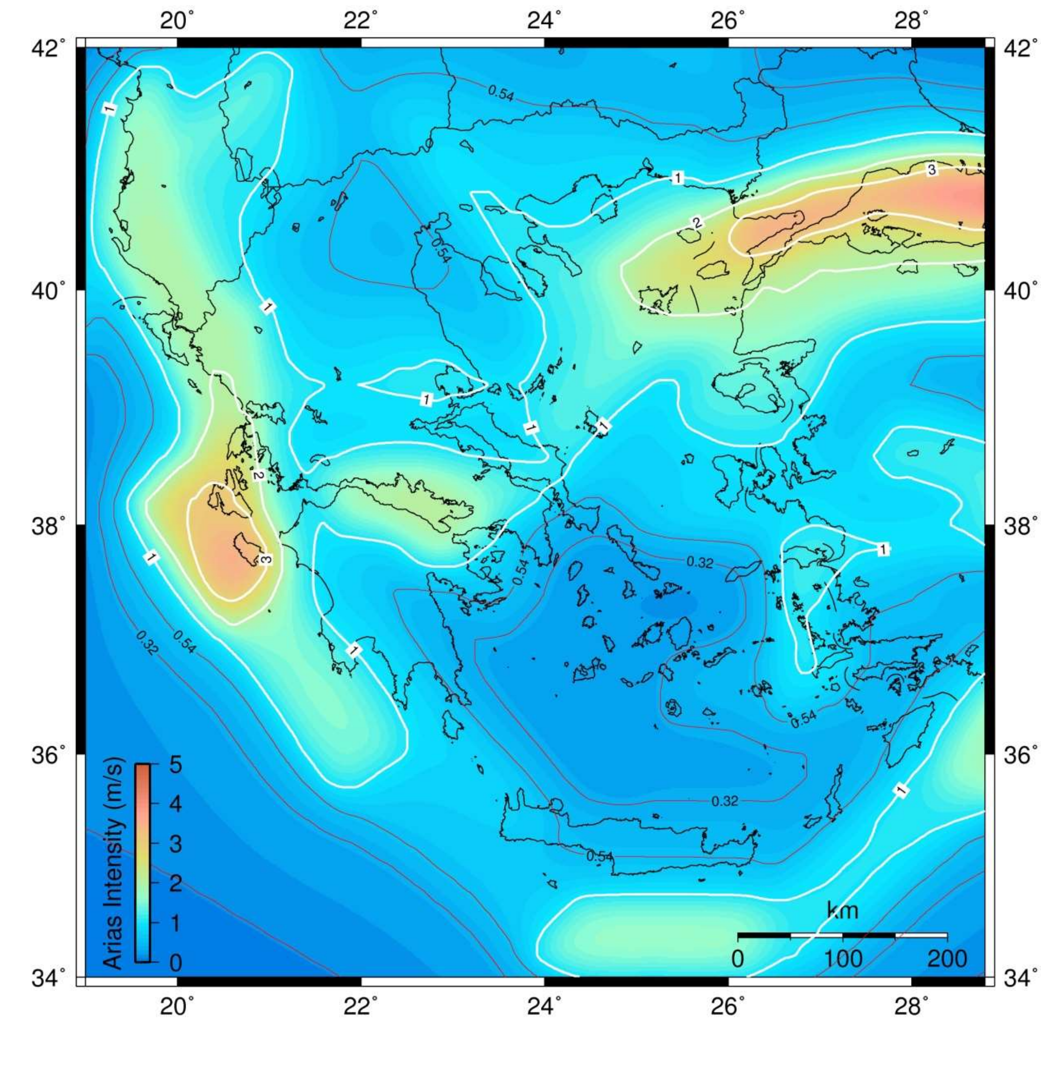

Figure 3b. Arias intensity values with 90% probability of not being exceeded in 50 years (475 years return period) for (b) soil site conditions.

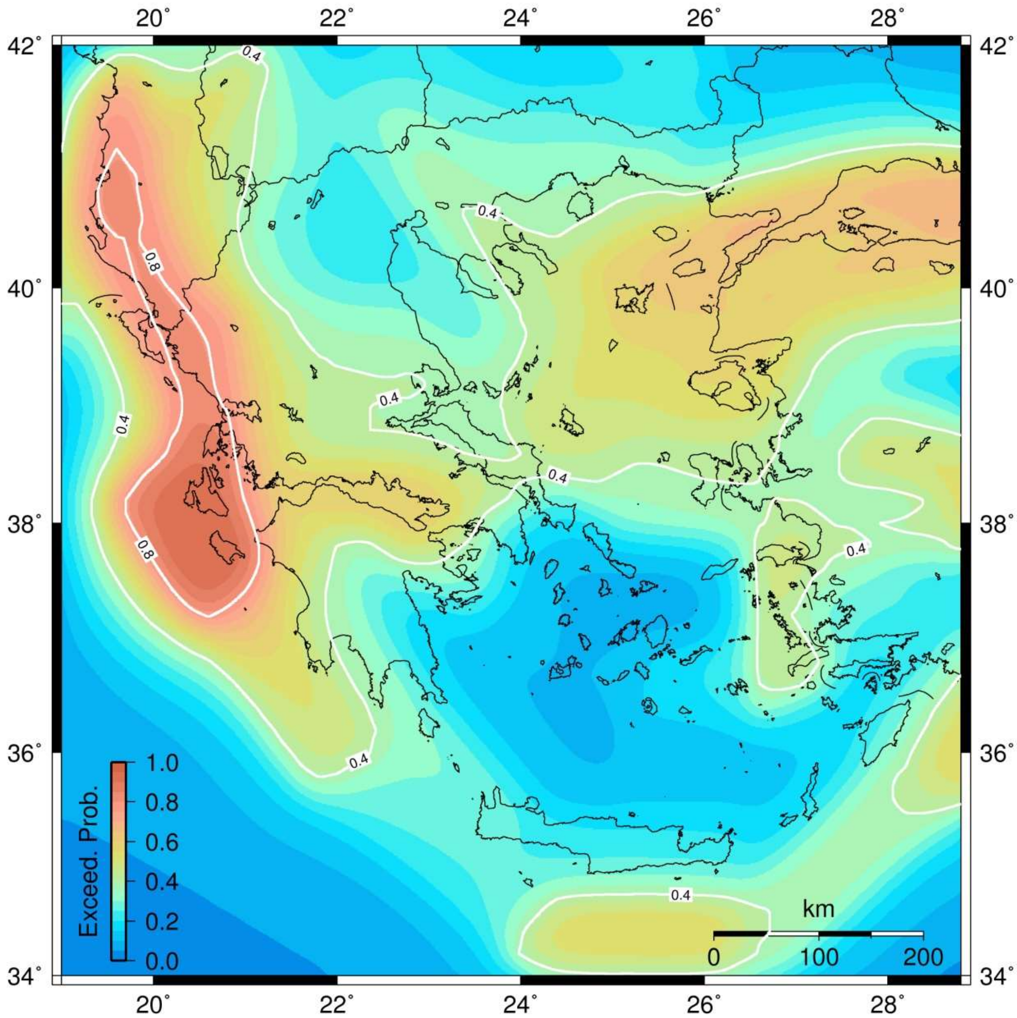

Figure 4a. Probabilities of exceedance in 50 years of Arias intensity thresholds equal to (a) 0.11 for rock site conditions.

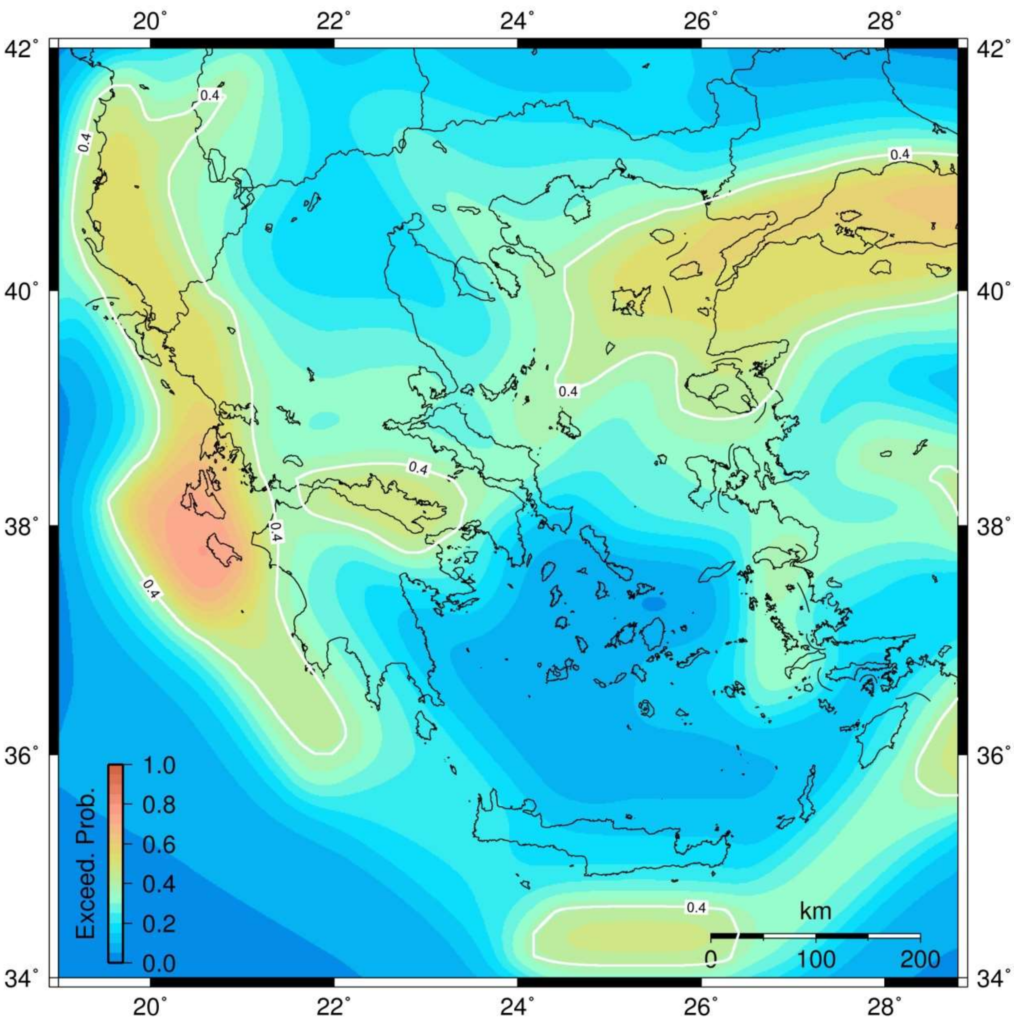

Figure 4b. Probabilities of exceedance in 50 years of Arias intensity thresholds equal to (b) 0.32 m/s for soil type conditions.

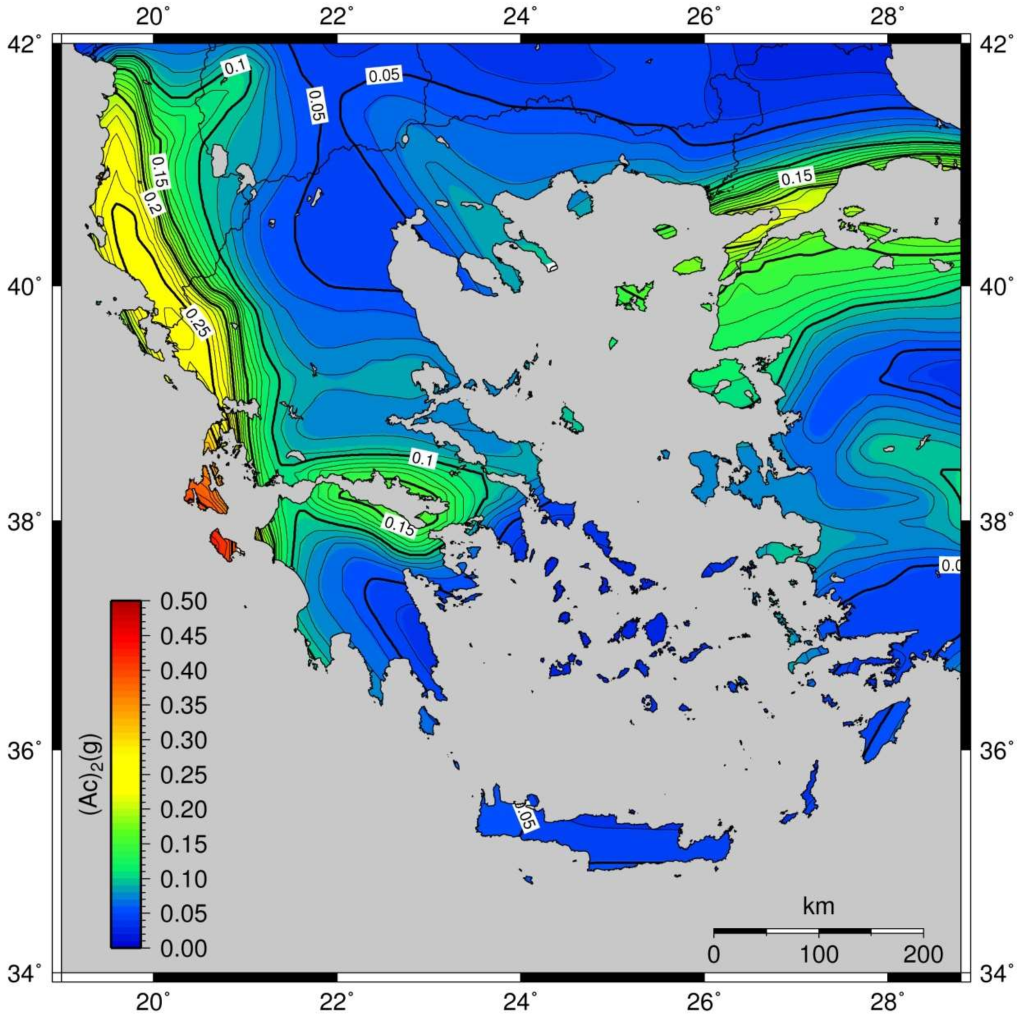

Figure 5a. Strength demand, expressed by critical acceleration $(A_c)_x$, requested to slopes in order to keep within 10% the probability of the occurrence of events causing, in a time span of 50 years, the exceedance of Newmark's displacement thresholds x equal to (a) 2 cm on rock slopes.

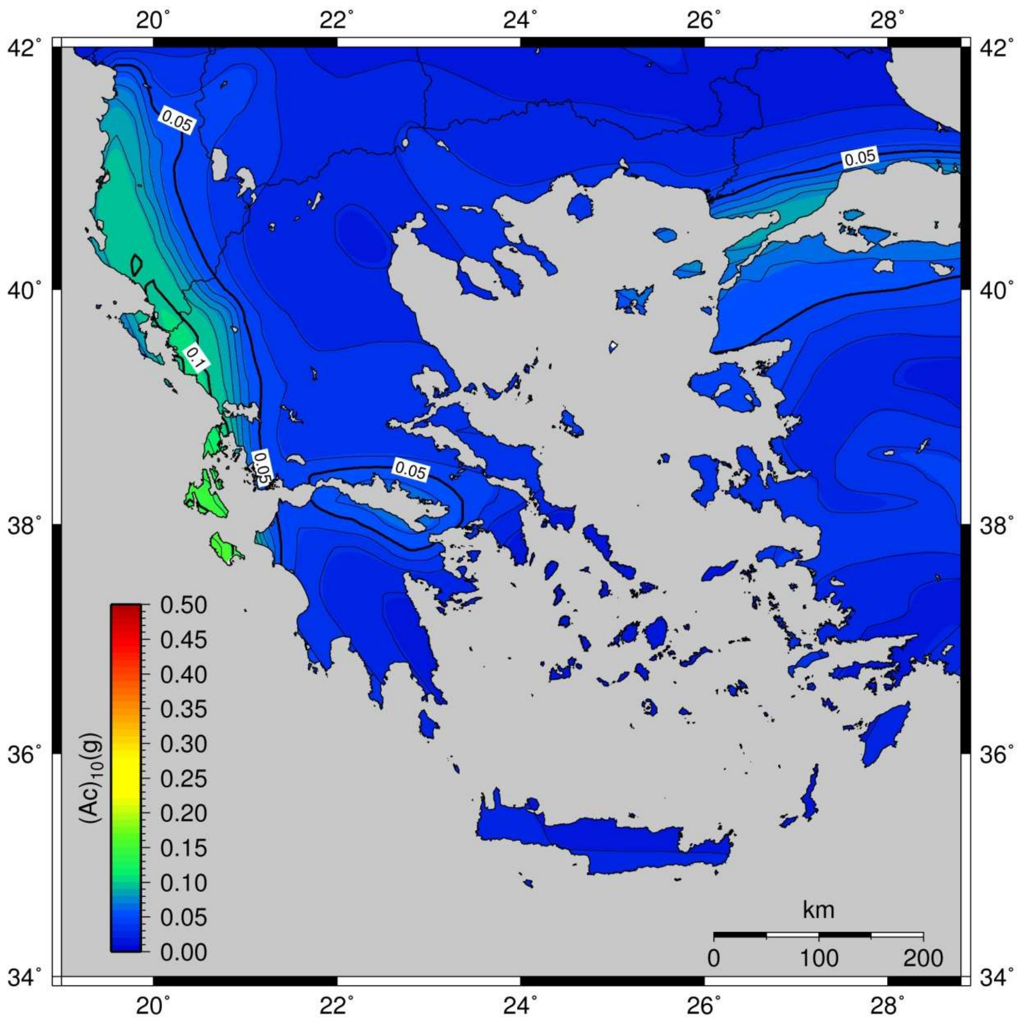

Figure 5b. Strength demand, expressed by critical acceleration $(A_c)_x$, requested to slopes in order to keep within 10% the probability of the occurrence of events causing, in a time span of 50 years, the exceedance of Newmark's displacement thresholds x equal to (b) 10 cm in soil slopes.

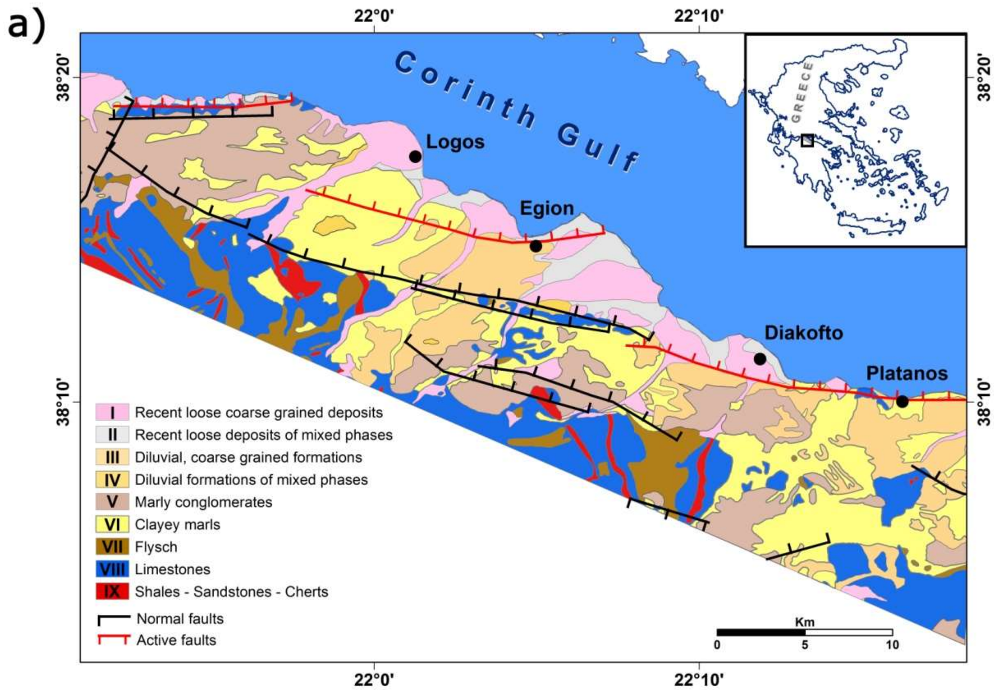

Figure 6. (a) Simplified engineering geological map with major faults (after Kokkalas and Koukouvelas, 2005) of the study area (marked by the thick-line rectangle in the inset box).

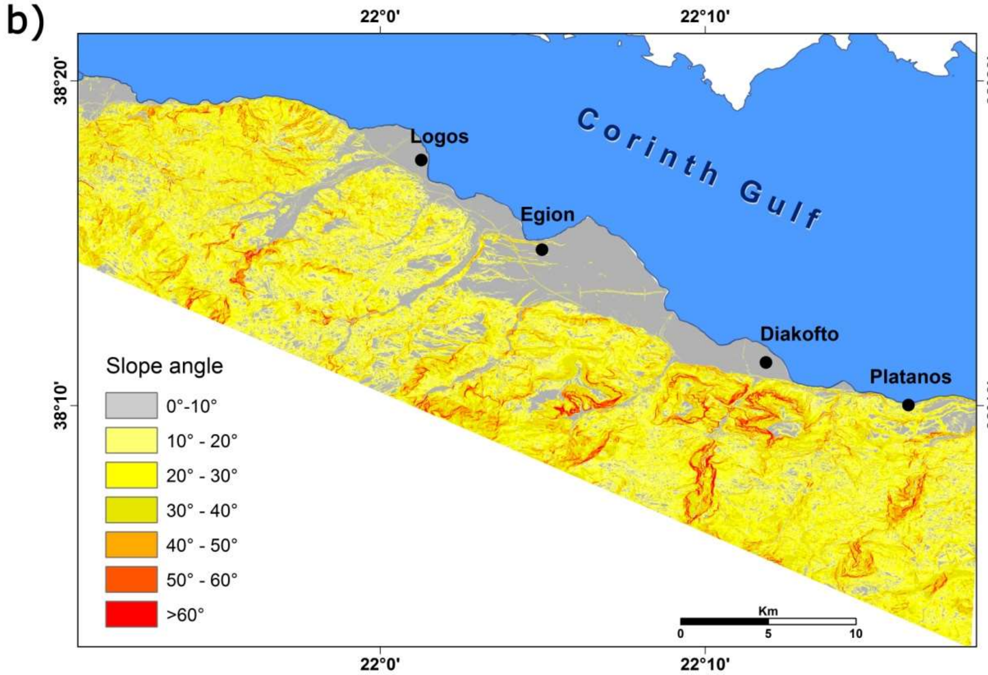

Figure 6. (b) Slope map created from Digital Surface Model.

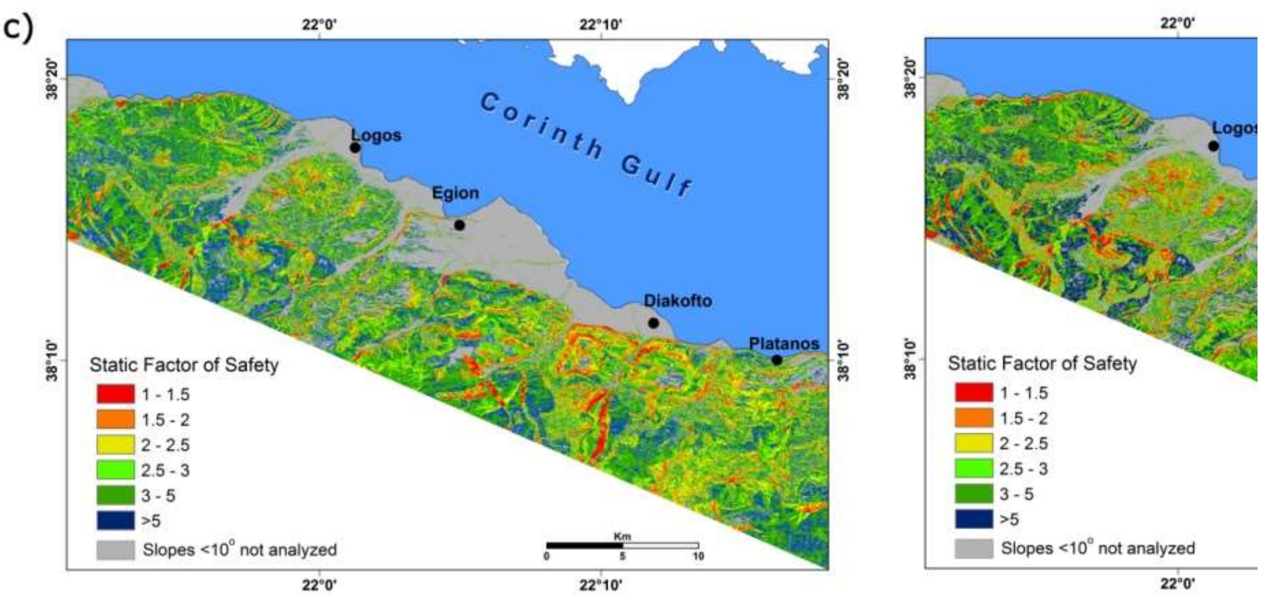

Figure 6. (c) Static factor of safety maps produced by applying equation (4) to raster data layers for situations expected in dry (left) and wet season (right) as discussed in text.

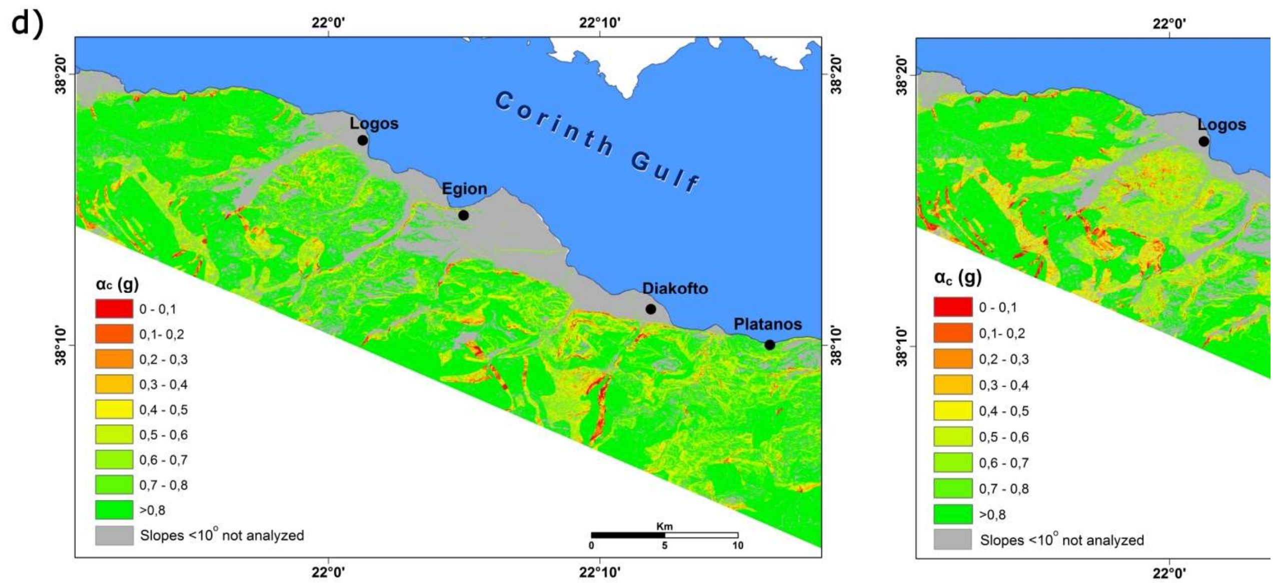

Figure 6. (d) Distribution of the critical acceleration values obtained from combining the static factor of safety layer with the slope angle layer according to equation (6) for dry (left) and wet (right) season.

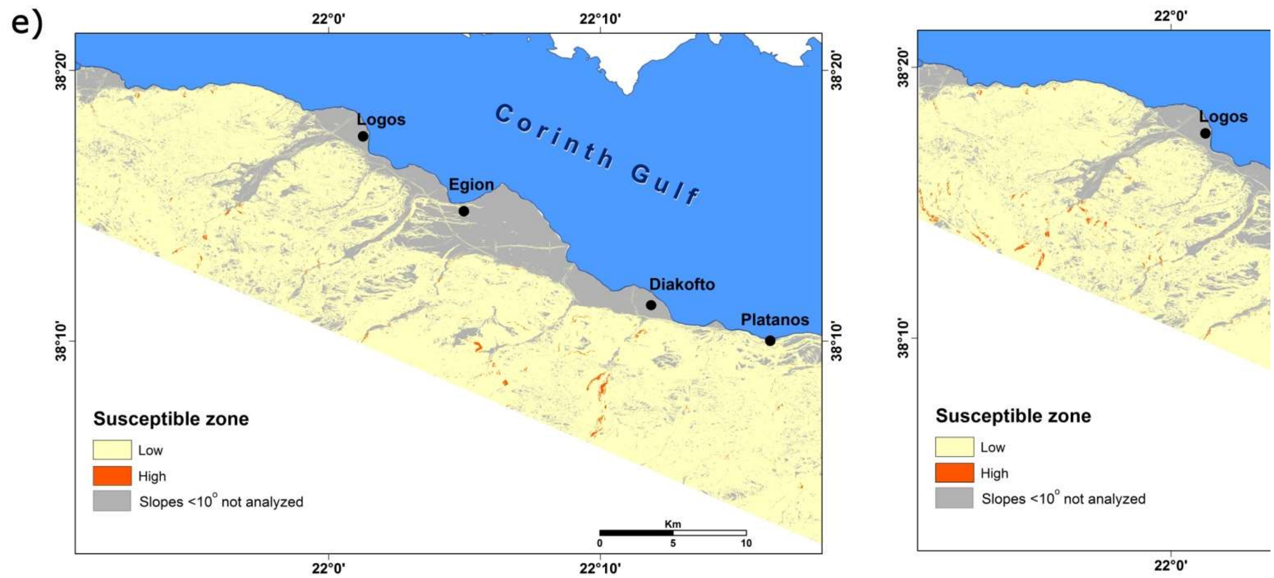

Figure 6. (e) Map showing the locations where the actual α_c values are below the calculated $(A_c)_\chi$ values, indicating the slopes that have a significant probability of failing under seismic action in the future for dry (left) and wet (right) season.